Research Article

Bo Li* and Jayanth Kanugo

Super-structured photonic crystal fiber Bragg grating biosensor image model based on sparse matrix

https://doi.org/10.1515/phys-2018-0091
Received Aug 26, 2018; accepted Sep 23, 2018

Abstract: Fiber grating (FBG) is an important optical device of fiber, which is widely used in optical fiber communication and sensing. At the present stage, the fiber grating is almost prepared in the static state of the fiber, and then the grating is welded into the fiber grating array or network. With the continuous improvement of the application effect of fiber grating, has become one of the most promising, representative and fastest developing fiber passive devices. In this paper, fiber grating is classified according to the refractive index distribution of grating axis. The central wavelength of Bragg fiber grating is modulated by using external parameters (temperature or stress strain). The wave equation of insulating medium is obtained by the reflection characteristic and coupling mode theory of fiber grating. Using sparse matrix model of nerve action potential signal with wavelet decomposition layers, nerve action potential signal reconstruction of the relative error between the value and the original value contrast found that reconstructed and original signals are very close. Good results have been obtained for the sampling reconstruction of the filtered high signal-to-noise ratio neural action potential signal. Researchers have conducted extensive and in-depth research on fiber grating sensing technology, and achieved gratifying results. But with the of the engineering application of technical requirements, they need real-time monitoring. Due to the cross sensitivities of fiber grating, it became the bottleneck of multiple parameter measurement.

Keywords: Sparse matrix; Reflection characteristics, PCF Bragg grating sensor; Fiber grating

PACS: 02.30.Cj, 02.50.Fz, 42.70.Qs

***Corresponding Author: Bo Li:** East China Jiaotong University, Information Engineering School, Nanchang, Jiangxi, China, 330013; Email: libo_jiaoda@126.com

Jayanth Kanugo: Computer Science Department, University of Missouri-Columbia, Columbia, United States of America

1 Introduction

The fiber grating uses the photosensitivity of the fiber material to form a spatial phase grating in the core [1–3].

It has a set of vertical reflection peaks and it can be used as a comb filter. Besides, it has potential applications in multi-wavelength fiber lasers. The essence of the fiber grating is to form in the core (wavelength characteristics of Bragg scattering using a spatial phase grating) a narrow-band (projection or reflection) filter. Fiber gratings are made using photosensitivity in optical fibers [4, 5]. The so-called photosensitivity in an optical fiber means that the refractive index of the optical fiber will change with the spatial distribution of the intensity of the light when the laser passes through the doped fiber. The essence of the spatial phase grating formed in the core is the formation of a narrowband filter or mirror in the core [6]. With this feature, many unique fiber optic devices can be manufactured. These devices have a wide range of reflection bandwidth, small additional loss, small size, easy to couple with the optical fiber, compatible with other optical devices into one, without the impact of environmental dust and a series of excellent performance.

With the increasing application of fiber gratings, the types of fiber gratings are also increasing. According to the distribution of refractive index along the axial direction of the grating, the ultraviolet-written fiber grating can be divided into a uniform fiber grating and a non-uniform fiber grating [7]. The uniform fiber grating refers to a fiber grating in which the core refractive index variation amplitude and refractive index variation period (also referred to as the period of the fiber grating) are all constant along the fiber axis, such as a uniform fiber Bragg grating (period of refractive index change is generally of 0.1 um) and uniform long-period fiber grating (period of refractive index change is generally the order of 100 um); Non-uniform fiber grating refers to the core refractive index varies in amplitude or refractive index varies along the fiber's axial direction. In 1978, K. O. Hill *et al.* first used the standing wave writing method to fabricate the first fiber grating in

erbium-doped fiber. After more than 20 years of development, it has broad application prospects in fields such as optical fiber communication and optical fiber sensing [8–10]. With the continuous improvement of the manufacturing technology of fiber gratings, the photosensitivity of optical fibers has been gradually improved, and various kinds of special gratings have come out one after another. Some applications of fiber gratings have reached the commercialization level. With increasing application results, FBG has become one of the most promising, most representative and fastest-developing fiber-optic passive devices currently available. FBG-based sensing technologies have emerged in recent years, fully demonstrating advantages. However, FBG sensing technology is still in a stage of rapid development. It can be predicted that with the commercialization of FBG sensors, continuous improvement of performance, fiber gratings will show great vitality in the field of sensing, and play an important and irreplaceable role in national defense and national economic construction. Significance statement: This study the superstructured photonic crystal fiber bragg grating biosensor image model based on sparse matrix that can be beneficial for the field of optical fiber sensing technology with its unique advantages.

2 Methods and principles

2.1 Sparse matrix model of neural action potential signals

Nerve action potential is a record of when a neuron is active [11]. It contains the most critical information about neuronal activity. Similar to other bioelectrical signals, neural action potentials can be sparse under orthogonal wavelet basis. Using this feature, a sparse matrix of neural signals can be constructed in the wavelet domain.

The construction of the sparse matrix is based on the Mallat algorithm of the discrete wavelet transform (DWT). The wavelet filter is used to decompose the signal [12]. The specific process can be expressed by the following formula (1):

$$\begin{cases} A_0\left[f(t)\right] = f(t) \\ A_j\left[f(t)\right] = \sum_k H(2t-k)A_{j-1}\left[f(t)\right] \\ D_j\left[f(t)\right] = \sum_k G(2t-k)A_{j-1}\left[f(t)\right] \end{cases} \tag{1}$$

In equation (1), t is the discrete time sequence number, $t = 1, 2, L, N$; $f(t)$ is the original signal; j is the number of layers, $j = 1, 2, L, J$, where $J = log_2 N$. H, G is the wavelet decomposition filter in the time domain, which is actually the filter coefficient; A_j Ai is the wavelet coefficient of the signal $f(t)$ at the approximate part (*i.e.*, the low frequency part) of the $j-th$ layer, and D is the detail of the signal $f(t)$ at the $j-th$ layer.

The specific decomposition process can be represented by Figure 1 and Figure 2.

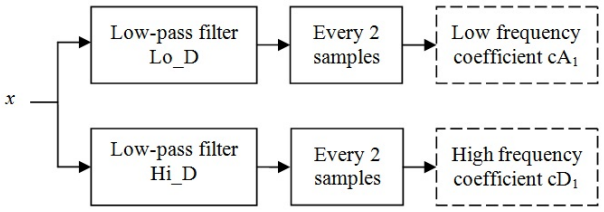

Figure 1: One-layer wavelet decomposition

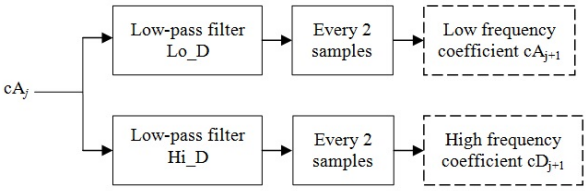

Figure 2: Multilayer wavelet decomposition

2.2 Optical mask distribution expression

Light through the mask, the light field distribution can be expressed as the following formula (2):

$$E(x) = 1 \bullet t_1(x) \bullet t_2(x) \tag{2}$$

Here, $t_1(x)$ and $t_2(x)$ are the transmittances of light transmitted through the amplitude mask and the phase mask, respectively. They can be expressed as the following formula (3):

$$t_1(x) = \begin{cases} 0 & -d/2 \le x \le a/2 \\ 1 & -a/2 \le x \le a/2 \\ 0 & a/2 \le x \le d/2 \end{cases} \tag{3}$$

$$t_2(x) = \begin{cases} \exp j\phi_1 & x + (2J+1)\Lambda/2 < \Lambda/2 \\ \exp j\phi_2 & x - J\Lambda/2 < \Lambda/2 \end{cases}$$

Where d is the period of the amplitude mask; a is the width of the tooth of the amplitude mask; L is the total length of the grating; $J = 0, \pm1, \pm2, \cdots$, Λ is the period of the phase mask. When the phase is produced, expanding the

formula (1) with Fourier series, the formula (1) can be expressed as the following formula (4):

$$E(x) = \sum_{n=-\infty}^{+\infty} A_n \exp\left(j\frac{2\pi nx}{d}\right) \sum_{n=-\infty}^{+\infty} C_m \exp\left(j\frac{2\pi mx}{\Lambda}\right) \quad (4)$$

Where, $A_n = \int_{-d/2}^{d/2} t_1(x)\exp\left(-j\frac{2\pi nx}{d}\right)\mathrm{d}x$; $C_m = \int_{-\Lambda/2}^{\Lambda/2} t_2(x)\exp\left(-j\frac{2\pi mx}{d}\right)dx$.

Equation (4) is the expression of the light field distribution of the ultraviolet laser after the periodic square wave modulation phase mask.

2.3 Principle and calculation of fiber Bragg grating reflection characteristics

Fiber Bragg grating is a waveguide with periodically varying refractive index. From coupled-mode theory, it can be seen that when the waveguide is disturbed periodically, it will lead to the coupling of propagation modes. Fiber Bragg grating sensing principle diagram was shown in Figure 3.

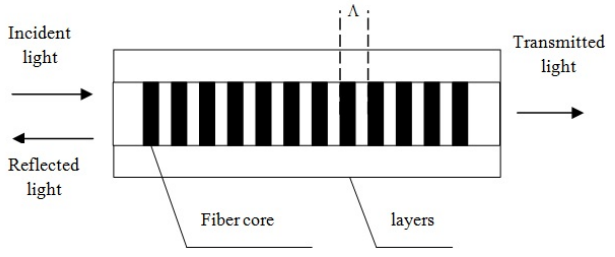

Figure 3: Fiber Bragg grating sensing principle diagram

Maxwell's equations can be expressed as the following Equations (5) and (6):

$$\nabla \times \overline{H} = \overline{J} + \frac{\partial}{\partial t}\left(\varepsilon_0 \overline{E} + \overline{P}\right) \quad (5)$$

$$\nabla \times \overline{E} = -\frac{\partial}{\partial t}(\mu \overline{H}) \quad (6)$$

For optical waveguides, there is no free charge, so $\overline{J} = 0$. Equations (5) and (6), the wave equation of insulating medium can be, the expression can be written as the following Equation (7):

$$\nabla^2 \overline{E}(\partial \overline{r}, t) = \mu\varepsilon_0 \frac{\partial^2 \overline{E}(\overline{r}, t)}{\partial t^2} + \mu \frac{\partial^2}{\partial t^2}\overline{P}(\overline{r}, t) \quad (7)$$

Due to the non-uniformity of the medium fluctuation, it can be considered as perturbation, and the polarization intensity can be expressed as the following Equation (8):

$$\overline{P}(\overline{r}, t) = [\varepsilon(\overline{r}) - \varepsilon_0]\overline{E}(\partial \overline{r}, t) + \overline{P}_{\text{Perturbation}}(\overline{r}, t) \quad (8)$$

Substituting (8) into (7), we can obtain the following equation (9):

$$\nabla^2 \overline{E}_y - \mu\varepsilon \frac{\partial^2 \bar{E}_y}{\partial t^2} = \mu \frac{\partial^2}{\partial t^2}[\bar{P}_{\text{Perturbation}}(\overline{r}, t)] \quad (9)$$

E_x and E_z are similar. For the TE mode, if you omit the guided mode and the radiation mode coupling, there is the following equation (10):

$$E_y(r, t) = \frac{1}{2}\sum_m A_m(z) E_y^{(m)}(x) e^{i(\omega t - \beta_m z)} + c.c. \quad (10)$$

where m is the number of the inherent mode, $c.c.$ is the complex conjugate, and the inherent mode field satisfies the non-disrupting sex wave equation. The non-disrupting sex wave equation can be expressed as following:

$$\left(\frac{\partial^2}{\partial x^2} - \beta_m^2\right) E_y^{(m)}(r) + \omega^2 \mu\varepsilon(r) E_y^{(m)}(r) = 0 \quad (11)$$

where $\varepsilon(r) = \varepsilon_0 n^2(r)$, $n(r)$ is the medium refractive index. Substituting (10) into (11), there is the following Equation (12):

$$\begin{aligned} & e^{i\omega t}\sum_m \left[\frac{A_m}{2}\left(-\beta_m^2 E_y^{(m)}\right.\right. \\ & \left. + \frac{\partial^2 E_y^{(m)}}{\partial x^2} + \omega^2\mu\varepsilon(r) E_y^{(m)}\right) e^{i\beta_m z} \\ & \left. + \frac{1}{2}\left(2i\beta_m \frac{dA_m}{dz} + \frac{d^2 A_m}{dz^2}\right) E_y^{(m)} e^{i\beta_m z}\right] + c.c. \\ & = \mu \frac{\partial^2}{\partial t^2}[P_{\text{Perturbation}}(r, t)] \end{aligned} \quad (12)$$

The sum of the first three terms of the equation is equal to zero, and the slow amplitude changes are similar. Omitting the second derivative, because the second derivative satisfies the following Equation (13), we get:

$$\left|\frac{d^2 A_m}{dz^2}\right| \ll \beta_m \left|\frac{dA_m}{dz}\right| \quad (13)$$

Substituting (13) into (12), there is the following Equation (14):

$$\begin{aligned} & \frac{dA_s^-}{dz} e^{i(\omega t + \beta_m z)} - \frac{dA_s^+}{dz} e^{i(\omega t + \beta_m z)} - c.c. \\ & = -\frac{i}{2\omega}\frac{\partial^2}{\partial t^2}\int_{-\infty}^{+\infty} [\bar{P}_{\text{Perturbation}}(\overline{r}, t)] E_y^{(x)} dx \end{aligned} \quad (14)$$

Where superscript – and + respectively represent propagation in the -z direction and the +z direction. The perturbation of the dielectric constant can be expressed as the periodic fluctuation of refractive index, which can be expressed as the following Equation (15):

$$\overline{P}_{\text{Perturbation}}(\overline{r}, t) = \Delta n^2(\overline{r})\varepsilon_0 \overline{E}(\overline{r}, t) \quad (15)$$

Since $\Delta n^2(\vec{r})$ is a scalar, as can be seen from Equation (8), the periodic structure can only couple the TE mode to the TE mode or the TM mode to the TM mode. However, it cannot couple the TE mode.

For the TE mode propagation, substitute (10) into (15) and (14), there is the following Equation (16):

$$\frac{dA_s^-}{dz}e^{i(\omega t+\beta_m z)} - \frac{dA_s^+}{dz}e^{i(\omega t+\beta_m z)} - c.c. \tag{16}$$
$$= -\frac{i\varepsilon_0}{4\omega}\frac{\partial^2}{\partial t^2}\sum_m\left[A_m\int_{-\infty}^{+\infty}\Delta n^2(x,z)]E_y^{(m)}(x)E_y^{(s)}(x)dxe^{i(\omega t+\beta_m z)} + c.c.\right]$$

Suppose the period of perturbation $\Delta n^2(x,z)$ is Λ, and $\frac{l\pi}{\Lambda} \approx \beta_s$, where l is the integer. So the Equation (17) can be obtained, which can be expressed as the following:

$$\Delta n^2(x,z) \approx \Delta n^2(x)\sum_{j=-\infty}^{+\infty} a_j e^{\left(\frac{i2j\pi}{\Lambda}\right)z} \tag{17}$$

Substituting (17) into (16), there is:

$$\frac{dA_s^-}{dz} = -\frac{i\varepsilon_0}{4\omega}A_s^+\int_{-\infty}^{+\infty}\Delta n^2(x)]\left[E_y^{(s)}(x)\right]^2 dxe^{i\left(\frac{2l\pi}{\Lambda}-\beta_s\right)} \tag{18}$$

Then the coupling equation by backward wave and forward wave at l-th harmonic can be expressed as the following Equation (19):

$$\frac{dA_s^-}{dz} = K_c A_s^+ e^{-i2(\Delta\beta)z} \tag{19}$$

Similarly, there is the following Equation (20)

$$\frac{dA_s^+}{dz} = K_c A_s^- e^{i2(\Delta\beta)z} \tag{20}$$

In the Equation (20), K_c and $\Delta\beta$ can be expressed as the following forms:

$$K_c = -\frac{i\omega\varepsilon_0}{4}a_t\int_{-\infty}^{+\infty}\Delta n^2(x)]\left[E_y^{(s)}(x)\right]^2 dx \tag{21}$$

$$\Delta\beta \equiv \beta_s - \frac{l\pi}{\Lambda} \equiv \beta_s - \beta_0 \tag{22}$$

Where K_c is called as the coupling coefficient. Equations (19) and (20) are the coupled mode equations for the forward and backward modes propagating in the periodic waveguide. Due to the agreement of two modes, so the power of these two modes is conserved.

For fiber Bragg grating, the waveguide structure is shown in Figure 4. Grating length is L, the grating period is Λ. The amplitude of light from the incident fiber, the amplitude of the backward wave at the boundary is 0. Assume that the fiber Bragg grating distribution is a strict sine function, the refractive index can be expressed as

$$n(z) = \overline{n} + \Delta n(z) = \overline{n} + \delta n\sin(\frac{2\pi z}{\Lambda}) \tag{23}$$

The coupling coefficient of the grating is $K = \frac{\pi\delta n\eta}{\lambda_B}$, where η is the coefficient related to the mode energy in the remaining core. Here $\eta = -V^2$ is approximated as the value of the fiber, V characterizes the modulus of the fiber transmission. Solving for Equations (19) and (20), the Equations (24) and (25) can be obtained:

$$A_s^-(z)e^{i\beta z} \tag{24}$$
$$= A_s^+(0)\frac{iKe^{i\beta z}}{-\Delta\beta\sinh(SL) + iS\cosh(SL)}\sinh\left[S(z-l)\right]$$

$$A_s^-(z)e^{i\beta z} = A_s^+(0)\frac{e^{-i\beta z}}{-\Delta\beta\sinh(SL) + iS\cosh(SL)} \tag{25}$$
$$\left\{\left(\Delta\beta\sinh\left[S(z-l)\right] + iS\cosh\left[S(z-l)\right]\right)\right\}$$

Where $S = \sqrt{|K|^2 - \Delta\beta^2}$, so the fiber Bragg grating reflectivity is obtained from (24) and (25), which can be expressed as:

$$R = \begin{cases}\frac{K^2\sinh^2(SL)}{\Delta\beta^2\sinh^2(SL)+S^2\cosh^2(SL)} & (K^2 > \Delta\beta^2)\\ \frac{K^2\sin^2(SL)}{\Delta\beta^2-K^2\cos^2(SL)} & (K^2 < \Delta\beta^2)\end{cases} \tag{26}$$

When the incident light wavelength is equal to the center wavelength of the fiber Bragg grating [Bragg wavelength]. $\Delta\beta = 0$, there is:

$$\lambda_B = 2n_{eff}\Lambda \tag{27}$$

$$R(\lambda_B) = \tanh^2(KL) \tag{28}$$

Where n_{eff} is called as the core effective refractive index.

Results and discussion

2.4 Nodes / edge mixed triangular units

The basic idea of finite element method is to separate the continuous solution area into a set of finite combinations, which are connected together in a certain way. Because the elements can be combined in different ways of joining and the elements themselves can have different shapes, the complex solution domain of geometric shapes can be modeled.

Figure 5(a) and (b) a typical triangular unit, expressed with e. The coordinates of the i-th vertex is $(x_i, y_i)(i$ =

1, 2, 3). The longitudinal field component is represented by E_{zi}^e. The edge length of the edge is expressed as l_i^e. The magnitude of the tangential field in the direction of the edge. The area of the triangle is expressed as Δ^e, which can be expressed as:

$$\Delta^e = \frac{1}{2}\begin{vmatrix} 1 & x_1^e & y_1^e \\ 1 & x_2^e & y_2^e \\ 1 & x_3^e & y_3^e \end{vmatrix} \quad (29)$$

Define the area coordinates of the triangle as $L_i^e = \Delta_i^e/\Delta^e$, where Δ_i^e is the value of the determinant obtained after the i-th row of the determinant. It has been replaced. Among them, the longitudinal field component is expressed as:

$$E_z^e(x,y) = \sum_{i=1}^{3} L_i^e E_{zi}^e = \left\{L^e\right\}^T \left\{E_z^e\right\} = \left\{E_z^e\right\}^T \left\{L^e\right\} \quad (30)$$

is the column vectors; superscript of Trepresents vector transpose. The horizontal field component can be expressed as:

$$E_t^e = \sum_{i=1}^{3} N_{ti}^e E_{ti}^e = \left\{N_t^e\right\}^T \left\{E_t^e\right\} = \left\{E_t^e\right\}^T \left\{N_t^e\right\} \quad (31)$$

Where, $N_{1t}^e = (L_1^e \parallel L_2^e - L_2^e \parallel L_1^e)l_1^e$,$N_{2t}^e = (L_2^e \parallel L_3^e - L_3^e \parallel L_2^e)l_2^e$.

On the basis of Figure 5, it keeps the air filling rate constant. When the hole spacing, the change tendency of waveguide dispersion curve in the wave band of interest, just as shown in Figure 6. As can be seen from Figure 4, not only the slope of the curve has changed, but also the curve has shifted. When the ratio of a/Λ is constant and the inter-hole spacing is increased, the curve (chromatic dispersion zero point) moves toward the long wavelength while the slope becomes smaller. When the ratio of a/Λ is constant and the inter-hole spacing decreases, the curve shifts toward the short wavelength move. The accuracy of this method is much higher than that of conventional fiber optic biosensors and photonic crystal fiber biosensors [13, 14]. This is also the main reason for the application of superstructure photonic crystal fibers based on biosensor image models [15, 16].

Due to the periodic change the refractive index of fiber core area, waveguide conditions changed, coupling phenomenon also occurred in a certain wavelength range, fiber Bragg grating is a narrow-band filter transmission (reflection).

According to the above rules, you can first adjust the aperture so that the 1st and 2nd zero waveguide dispersion curve shifted to 1.55 μm wavelength window. Since the material dispersion curve is approximately linear on

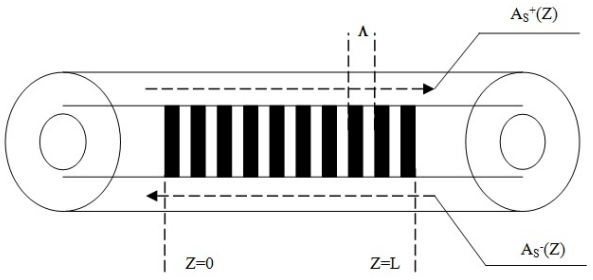

Figure 4: Fiber Bragg grating waveguide structure diagram

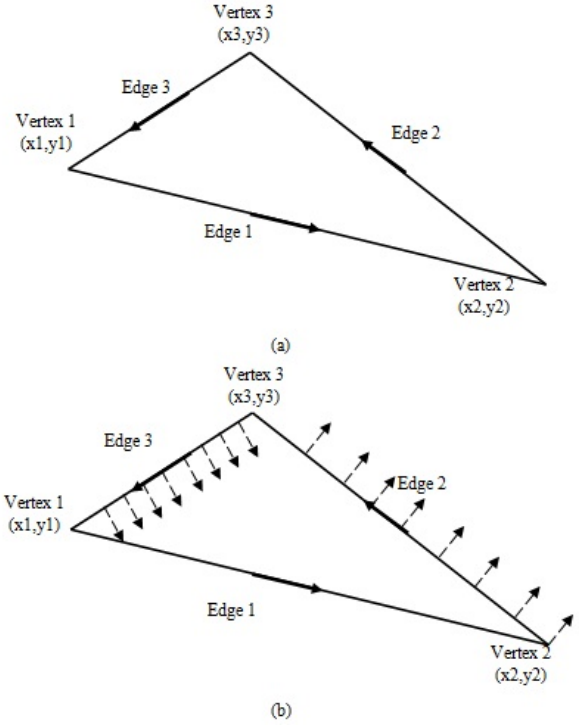

Figure 5: (a) Hybrid edge/ node elements with triangular shape (b) The vector expansion function corresponding to any edge (*e.g.* edge 1) has tangential element only this edge

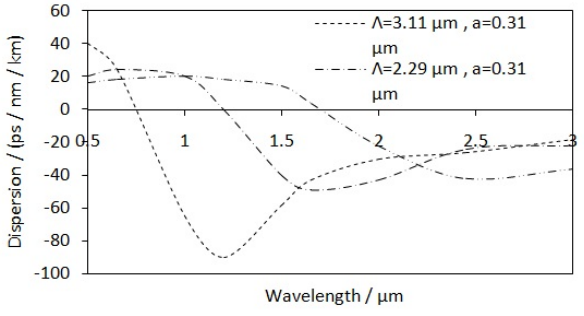

Figure 6: The effect of the pitch on waveguide dispersion while keeping air filling coefficient unchanged

this window, if the ratio of is kept constant and then the hole spacing is adjusted, the slope of the waveguide dispersion will increase or decrease. As a result, it is necessary to find suitable structural parameters. The material dispersion and the waveguide dispersion slope are approximately equal and the signs are opposite, so that the total dispersion is approximately zero. The numerical simulation structure is shown in Figure 7. In this case, the dispersion is ± 0.2 ps/km/nm in the 1550 ± 100 nm band with a dispersion slope of −0.003 ps/km/nm^2. The mode field Λ = 3.24 μm, the nonlinear coefficient γ = 15.8 W^{-1} · km^{-1}, which is much larger than that of conventional SMF. The zero-dispersion point is also located near the pump laser wavelength (1.55 μm). These data ensure that the parametric amplifier has a high gain and a large bandwidth.

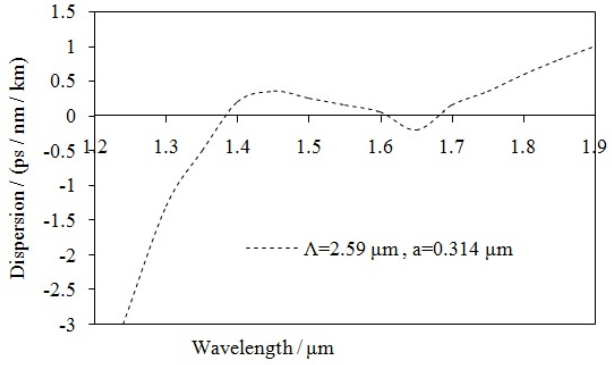

Figure 7: The near zero flatten dispersion characteristics of PCF near 1.55 μm

It can be seen that the relative error calculation values of the highest point (peak), lowest point (peak) and time course of the original signal and the reconstructed signal are relatively small, and basically less than 10%, all less than 15%. This shows that the reconstructed signal is very close to the original signal, that is, the method used in this paper achieves better results by sampling and reconstructing the neural action potential signal with high signal-to-noise ratio after filtering.

The fabrication process of chemical component fiber Bragg grating generally includes the steps of hydrogen loading, hydrogen diffusion and high temperature annealing. The degradation and regeneration of grating occur at high temperature annealing stage. The refractive index modulation reduced to 20%. The high temperature test process of chemical component fiber grating is shown in Figure 8. This kind of grating has excellent high temperature stability, able to work under the high temperature of environment. Similar to previous experimental studies [17–19], the amount of change in the measurement results of this study, the sensitivity of the refractive index. Both the curve variation law and the feature distribution have reached a high degree of agreement, thus ensuring the accuracy and effectiveness of the research results. This lays a theoretical foundation for the application of superstructure photonic crystal fiber Bragg grating in biosensor image [20].

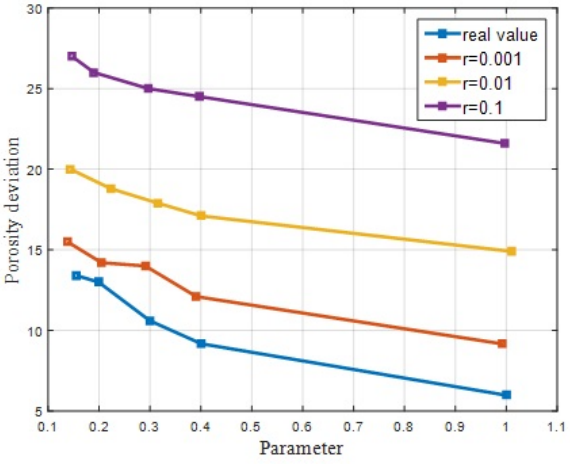

Figure 8: Chemical composition of optical fiber grating under refractive index modulation normalized decline curve

3 Conclusions

This study finds that the application of fiber grating sensor is a new subject and has a broad development prospect. That can be beneficial for large structure engineering, power engineering, geotechnical engineering, traffic engineering, mining engineering, blasting engineering, petrochemical industry, aerospace, biomedical, ships, oil exploration, and military weapons and equipment, etc. In this paper, the characteristics and basic principles of fiber grating are briefly introduced, and the application status of fiber grating sensing technology is analyzed. Then, according to the feature that the neural action potential can be sparse, the sparse matrix of neural signals can be constructed in the wavelet domain, and the signal can be decomposed by the wavelet filter. Furthermore, according to the principle of reflection characteristics of fiber grating, the wave equation of insulating medium is calculated from the coupled mode theory. Finally, under the condition of invariable in keeping the air filling factor, a comprehen-

sive analysis of the influence of pitch of waveguide dispersion, it is concluded that the hole spacing increases, the curve is zero to the long wavelength direction, and the slope has shrunk, and hole spacing and small curve move in the direction of short wavelength. Contrast nerve action potential signal reconstruction based on sparse matrix values and original values, that the smaller values of the relative error between them, that was very close to reconstruct signal and original signal, the method adopted by the after filtering by a high signal-to-noise ratio of nerve action potential signal sampling refactoring got good results. The study will help researchers identify key areas that many have been unable to explore. Although the research on fiber grating sensing technology in China is relatively late, it can be predicted that with the deepening of the research on fiber grating sensing technology, there will be a new breakthrough in its application. Therefore, a number of major projects will be launched in succession, and fiber grating sensing technology will provide an effective way for long-term stable and real-time online security monitoring of these projects.

Acknowledgement: This work was supported by Natural Science Foundation of China (No. 61863013), Key R & D projects of Jiangxi science and Technology Department of China (No. 20161BBE50091) and Science and Technology Foundation of Jiangxi Educational Committee of China (No. 150529).

References

[1] Liu Y., Zhang J., Model study of the influence of ambient temperature and installation types on surface temperature measurement by using a fiber bragg grating sensor, Sensors, 2016, 16.7, 975

[2] Sengupta S., Ghorai I., Swapan K., Biswas P., Design of superstructure fiber Bragg grating with efficient mode coupling for simultaneous strain and temperature measurement with low cross-sensitivity, IEEE Sensors Journal, 2016, 16.22, 7941-7949.

[3] Chen T., Experimental study on cross-sensitivity of temperature and vibration of embedded fiber Bragg grating sensors, Optoelectr. Lett., 2018, 14.2, 92-97.

[4] Zhou L., Liang D., Zeng J., The influence of temperature on the deuteration mechanism and experimental research of fiber grating sensor performance, China Laser, 2012, 39.4, 1-6.

[5] Chong S., Dye concentration determination with cross-sensitivity compensation, Sensors and Actuators B: Chemical, 2016, 226, 450-456.

[6] Rajan G., Experimental study and analysis of a polymer fiber Bragg grating embedded in a composite material, J. Lightwave Techn., 2014, 32.9, 1726-1733.

[7] Zhang D., Zheng Y., Research on cross-sensitivity problem of FBG temperature sensor, Journal of Atmospheric and Environmental Optics, 2016, 11.3, 226-233.

[8] Carlo M., Michele A., Rosaria D., Fiber Bragg Grating Measuring System for Simultaneous Monitoring of Temperature and Humidity in Mechanical Ventilation, Sensors, 2017, 17.4, 749.

[9] Hu J., Yang Y., Liu X., Based on gap fiber grating micro-gap and temperature measurement technology, China Laser, 2014, 41.11, 201-206.

[10] Liu S., Chen T., Li R., Study on the Effect of Paste Effect of Substrate FBG Temperature Sensor on Its Performance, Optoelectr. Laser, 2016, 27.7, 692-698.

[11] Liu Y., Guo Z., Zhang Y., Simultaneous measurement of single fiber grating pressure and temperature, China Laser, 2010, 27. 11, 1002-1006.

[12] Huang J., Zhou Z., Tan Y., Design and Experimental Study of a Fiber Bragg Grating Pressure Sensor, International Conference on Innovative Design and Manufacturing, August 13-15, 2014, Montreal Canada, Piscataway: IEEE, 2014, 217-221.

[13] Zhu D., Qin H., Analysis of Sampled Fiber Bragg Grating Based on the Photonic Crystal Theory, Semicond. Photonics & Techn., 2009, 39.3, 184-188.

[14] Geng D., Yang D., Zhang X., All-optical generation of microwave using a photonic crystal fiber Brillouin laser based on Bragg grating Fabry-Perot cavity, Microwave & Optical Techn. Lett., 2010, 50.3, 809-814.

[15] Liu H., Tan C., Zhu C., Multi-parameters measurement based on cascaded Bragg gratings in magnetic fluid-infiltrated photonic crystal fibre, Optica Acta Int. J. Optics, 2016, 64.8, 887-894.

[16] Rindorf L., Bang O., Sensitivity of photonic crystal fiber grating sensors: biosensing, refractive index, strain, and temperature sensing, J. Optic. Soc. Amer. B, 2007, 25.3, 310-324.

[17] Tan X., Geng Y., Li X., High-birefringence photonic crystal fiber Michelson interferometer with cascaded fiber Bragg grating for pressure and temperature discrimination, Optic. Engin., 2016, 55.9, 090508.

[18] Wang B., Huang Y., Research on characteristics of the twelve polygon photonic crystal fiber grating, Semicond. Optoelectr., 2014, 35.6, 1000-1003.

[19] Yiping W., Wang M., Huang X., In fiber Bragg grating twist sensor based on analysis of polarization dependent loss, Optics Express, 2013, 21.10, 11913-11920.

[20] Carpintero G., Balakier K., Yang Z., Microwave Photonic Integrated Circuits for Millimeter-Wave Wireless Communications, Lightwave Technology Journal, 2014, 32.20, 3495-3501.